

Latest KLOE-2 results on hadron physics

Dario Moricciani* *on behalf the KLOE-2 collaboration*

INFN-Sez. Roma "Tor Vergata", Via della Ricerca Scientifica 1, I-00133, Rome

E-mail: Dario.Moricciani@roma2.infn.it

We discuss recent results of the KLOE experiment at the ϕ factory DAΦNE. Precision measurements were obtained on i) Dalitz ϕ decays, $\phi \rightarrow \pi^0 e^+ e^-$ and $\phi \rightarrow \eta e^+ e^-$ and ii) the isospin-violating decay $\eta \rightarrow \pi^+ \pi^- \pi^0$, of interest for effective field theory of low-energy QCD.

*38th International Conference on High Energy Physics
3-10 August 2016
Chicago, USA*

*Speaker.

1. Introduction

The KLOE experiment at the Frascati ϕ -factory DAΦNE took most of the data in 2004-2006, with 2.5 fb^{-1} of integrated luminosity at the ϕ peak, and about 240 pb^{-1} at 1 GeV, 20 MeV below the resonance, for the analysis of dipion, dilepton production and γ - γ interactions. A new data taking campaign with an upgraded detector KLOE-2 is ongoing with the goal to record an integrated luminosity of 5 fb^{-1} by the end of 2017 to extend the experimental program of KLOE in kaon and hadron physics [1].

Recent results in hadronic physics concerning the measurement of π^0 and η coupling to photons will be described in the following. Meson to photon couplings and transition form factors, TFFs, are fundamental measurements in hadron physics, of interest for effective Lagrangians of low-energy QCD based on Chiral Perturbation Theory, ChPT[2, 3] and for studies of the transition regime from soft, non-perturbative QCD, to hard interactions, described by pQCD. The transition form factors for π^0 and η in the time-like region are provided by the measurements of i) the Dalitz decays (as $\eta \rightarrow \gamma e^+ e^-$), ii) $V \rightarrow P\gamma$ transitions (as $\phi \rightarrow \eta e^+ e^-$, $\phi \rightarrow \pi^0 e^+ e^-$, $\omega \rightarrow \pi^0 e^+ e^-$), while iii) meson production in γ - γ interactions (as $e^+ e^- \rightarrow e^+ e^- \gamma^* \gamma^* \rightarrow e^+ e^- \pi^0$) gives the coupling to space-like photons, of interest also for the evaluation of light-by-light contribution to the anomalous magnetic moment of the muon[4].

We obtained also the precision measurement of the Dalitz plot of the isospin-violating decay $\eta \rightarrow \pi^+ \pi^- \pi^0$, as discussed in sec.4.

2. $\phi \rightarrow \pi^0 e^+ e^-$

The $\phi \rightarrow \pi^0 e^+ e^-$ decays are identified from the reconstruction of i) two clusters in the calorimeter that were consistent with π^0 decays, and ii) two tracks of opposite charge in the drift chamber (DC). The origin of both, clusters and tracks, is close to beam interaction region, IR. The $e^+ e^-$ pairs are identified from time-of-flight measurements in the calorimeter. The excellent time resolution is in fact very effective to separate electron/positron pairs from muons and pions. The dominant background is constituted of radiative Bhabha scattering processes. The contamination from $\phi \rightarrow \pi^0 \gamma$ decays with photon conversion to $e^+ e^-$ pairs on the beam pipe (BP) or DC walls is suppressed by proper cuts on the distance between tracks and on the invariant mass, as measured at the BP and DC walls. The background contribution from QED process $e^+ e^- \rightarrow e^+ e^- \gamma \gamma$ is rejected by cuts on the energies and opening angles of both, track and neutral-cluster pairs[5].

The overall efficiency for the signal is 15.4%, as estimated by MonteCarlo simulation. It is higher, 19.5%, at low $e^+ e^-$ invariant masses and decreases to few percent at the highest value of momentum transfer considered in the analysis, $\sqrt{q^2} = 700 \text{ MeV}$. At the end of the analysis chain, 14670 events are selected, with a residual background contamination of $\sim 35\%$, equally divided between Bhabha's and $\phi \rightarrow \pi^0 \gamma$ decays (see fig. 1 left). In order to subtract the residual background from data, the $e^+ e^-$ invariant-mass spectrum is divided into 15 bins of increasing width. The distribution is fitted in each bin with the sum of two Gaussians, parametrizing the signal, and a third-order polynomial, for the background. Fit results are used for bin-by-bin subtraction of the background. The branching ratio is obtained from the background-subtracted $e^+ e^-$ mass spectrum taking into account bin-by-bin efficiency,

$$\text{BR}(\phi \rightarrow \pi^0 e^+ e^-) = \frac{\sum_i N_i / \varepsilon_i}{\sigma_\phi \times \mathcal{L}_{\text{int}} \times \text{BR}(\pi^0 \rightarrow \gamma\gamma)}, \quad (2.1)$$

where σ_ϕ is the effective ϕ production cross-section, $\sigma_\phi = (3310 \pm 120)$ nb, $\mathcal{L}_{\text{int}} = (1.69 \pm 0.01)$ fb $^{-1}$ [6] is the integrated luminosity, and $\text{BR}(\pi^0 \rightarrow \gamma\gamma)$ is taken from the world average in ref.[7]. N_i is the number of candidates and ε_i the efficiency. We get $\text{BR}(\phi \rightarrow \pi^0 e^+ e^-; \sqrt{q^2} < 700 \text{ MeV}) = (1.19 \pm 0.05^{+0.05}_{-0.10}) \times 10^{-5}$, where the first error is the combination of statistical and normalization uncertainties and the second is a systematic error due to analysis cuts and background subtraction. The branching ratio in the entire kinematical range, using the form factor of ref.[8] is: $\text{BR}(\phi \rightarrow \pi^0 e^+ e^-) = (1.35 \pm 0.05^{+0.05}_{-0.10}) \times 10^{-5}$.

In fig. 1, right, the results on $|F_{\phi\pi^0}(q^2)|^2$ are compared with three different theoretical predictions. The best agreement is obtained with the Unconstrained Resonant Chiral Theory (UChT), where NA60 data have been used as input to the model[8].

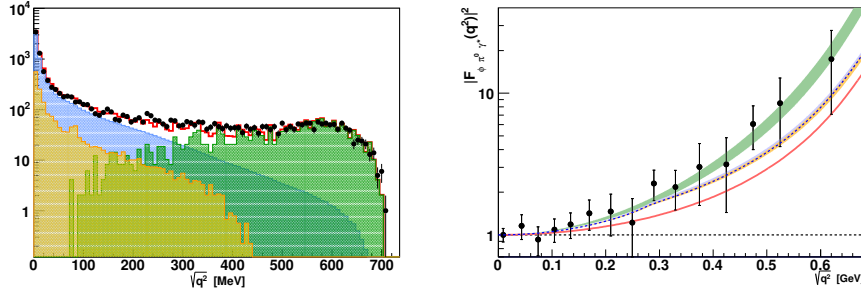


Figure 1: On the left: Data-MC comparison after all the analysis cuts for invariant-mass spectrum of e^+e^- . Black dots are data, solid red line is the sum of MC histogram components: signal (cyan), $\phi \rightarrow \pi^0\gamma$ background (orange) and radiative Bhabha scattering (green). On the right: comparison between the measurement of $|F_{\phi\pi^0}(q^2)|^2$ (black points) and theoretical predictions of ref.[3] (orange and cyan bands), ref.[9] (blue dashed line), ref. [8] (green band), and the one-pole VMD model (solid red line).

Transition form factors are usually presented by one-pole approximation, $F(q^2) = \frac{1}{1-q^2/\Lambda^2}$, and parametrized by the slope parameter, $b = \Lambda^{-2}$. We get $b_{\phi\pi^0} = (2.02 \pm 0.11)$ GeV $^{-2}$, to be compared with expectations from i) one-pole approximation, $b_{\phi\pi^0} = M_\phi^{-2}$, and ii) dispersive analysis[3], $b_{\phi\pi^0} = (2.52-2.68)$ GeV $^{-2}$.

3. $\phi \rightarrow \eta e^+ e^-$

Dalitz decays, $\phi \rightarrow \eta e^+ e^-$ have been studied selecting events with $\eta \rightarrow \pi^0\pi^0\pi^0$ on a sample of 1.7 fb $^{-1}$ of integrated luminosity. Events with two tracks of opposite sign and six neutral clusters from IR, are selected. Clusters in the final state have invariant mass consistent with the η mass. The e^+e^- pairs are identified from time-of-flight measurements, as in sec.2. Missing invariant mass, $M_{\text{recoil-}ee}$ is reconstructed from beam-beam and final-state e^+e^- momenta, and is used to identify $\phi \rightarrow \eta e^+ e^-$ candidates, selecting $536.5 \text{ MeV} < M_{\text{recoil-}ee} < 554.5 \text{ MeV}$. The contamination from $\phi \rightarrow \eta\gamma$ decays, mainly due to events with photon conversion to e^+e^- pairs on the beam pipe (BP) or DC walls, is suppressed by tracking back e^+ and e^- candidates and cutting on their invariant mass, M_{ee} , and distance as reconstructed at the BP and DC wall surfaces. M_{ee} distributions, after

cutting on $M_{recoil-ee}$, and at the end of the analysis chain, are shown in fig. 2, compared to MC expectations. Background contamination is concentrated at high masses and dominated by $\phi \rightarrow K_S K_L \rightarrow \pi^+ \pi^- 3\pi^0$ events with an early K_L decay.

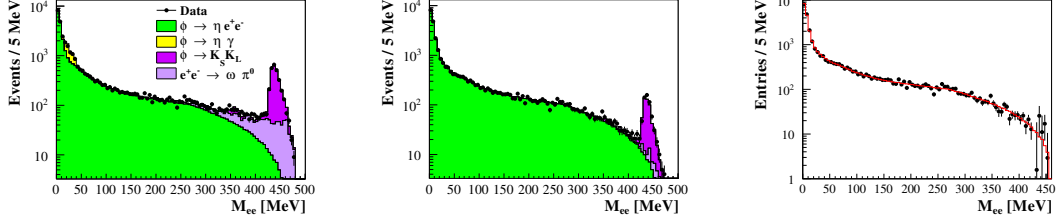


Figure 2: Data-MC comparison of M_{ee} distributions i) after $M_{recoil-ee}$ cut (left), and ii) at the end of the analysis chain (center). The MC-simulated sample of the signal corresponds to an integrated luminosity 100 times larger than experimental data. Right: fit to the M_{ee} spectrum after background subtraction, in logarithmic scale.

Signal selection efficiency is 10% at low masses and increases to $\sim 35\%$ at 460 MeV, following the increase with particle momentum of DC acceptance. A final sample of 30577 events is selected, with $\sim 3\%$ background contamination. The $\phi \rightarrow \eta e^+ e^-$, $\eta \rightarrow 3\pi^0$ candidates are 29625 ± 178 as obtained by bin-by-bin background subtraction on the M_{ee} spectrum. Branching ratio is given by: $BR(\phi \rightarrow \eta e^+ e^-) = \frac{\sum_i N_i / \epsilon_i}{\sigma_\phi \times \mathcal{L} \times BR(\eta \rightarrow 3\pi^0)}$, using i) bin-by-bin efficiency correction, ϵ_i , ii) the luminosity measurement obtained from very large angle Bhabha's [6], \mathcal{L} , and iii) the effective ϕ production cross section σ_ϕ that takes into account center of mass energy variations at 1% level, as measured on the same Bhabha sample. The effective cross section is $\sigma_\phi = (3310 \pm 120)$ nb, and the total integrated luminosity $\mathcal{L} = (1.68 \pm 0.01)$ fb $^{-1}$. The $BR(\eta \rightarrow 3\pi^0) = (32.57 \pm 0.23)\%$ was taken from the average of published measurements [7]. We obtain, $BR(\phi \rightarrow \eta e^+ e^-) = (1.075 \pm 0.007 \pm 0.038) \times 10^{-4}$, where systematics are dominated by the uncertainty on the normalization factors, i.e. luminosity, ϕ production cross section, and $\eta \rightarrow \pi^0 \pi^0 \pi^0$ branching fraction. The transition form factor, $F_{\phi\eta}(q^2)$ is obtained from a fit to the M_{ee} distribution with the function [10], the results are shown and compared with data in fig. 2, right. The result for the slope of the transition form factor is: $b_{\phi\eta} = (1.17 \pm 0.10_{-0.11}^{+0.07})$ GeV $^{-2}$. The modulus squared of the transition form factor, $|F_{\phi\eta}(q^2)|^2$ as a function of the $e^+ e^-$ invariant mass, is obtained by dividing bin-by-bin the M_{ee} spectrum of fig. 2, right, by the one from a MC sample generated with $F_{\phi\eta}^{MC} = 1$, after all analysis cuts [10]. Both measurements, the $BR(\phi \rightarrow \eta e^+ e^-)$, and the transition form factor slope are in agreement with VMD predictions [11], and with the SND and CMD-2 results [12, 13] that have been improved in precision by a factor of five.

4. Dalitz plot of η decay to $\pi^+ \pi^- \pi^0$

Three-body meson decays constitute a test bench for Chiral Perturbation Theory, effective field theory of low-energy QCD. In particular, $\eta \rightarrow \pi^+ \pi^- \pi^0$ decays have been used to study isospin breaking in strong interactions and to obtain constraints on the light quark masses. The issue with such process is the slow convergence of effective field theory, requiring the evaluation of NNLO terms to reach even a modest theoretical precision. Resummed ChPT [14] was developed to explicitly include uncertainties associated with such slow convergence of the perturbative

series, also to solve some tension between theory and experimental data on the pion differential kinematical distribution.

The usual parametrization of the Dalitz plot, i.e. the decay amplitude distribution $|A(s, t; u)|^2$, is used:

$$|A(s, t; u)|^2 = |A(s_0, s_0; s_0)|^2 (1 + ay + by^2 + dx^2 + fy^3 + gx^2y + \dots) \quad (4.1)$$

where $x = \sqrt{3} \frac{T_+ - T_-}{Q_\eta} = -\frac{\sqrt{3}}{2M_\eta Q_\eta} (t - u)$; $y = 3 \frac{T_0}{Q_\eta} - 1 = -\frac{3}{2M_\eta Q_\eta} (s - s_0)$, with $Q_\eta = T_0 + T_+ + T_- = M_\eta - 3M_\pi$. $T_{0,\pm}$ are kinetic energies of final states $\pi^{0,\pm}$.

Eq.4.1 is the Taylor expansion around the center of the Dalitz plot, $s = t = u = s_0$. C-invariance excludes terms with odd powers in x .

A precision measurement of the Dalitz plot density has been carried out, on the basis of 1.7 pb^{-1} . Two tracks of opposite curvature and three neutral clusters originated at the IR are required in the final state. The highest-energy photon, from the 2-body ϕ decay $\phi \rightarrow \eta \gamma_\phi$, is selected with $E_{\gamma_\phi} > 250 \text{ MeV}$. Discrimination against electron contamination from Bhabha scattering is achieved by means of time-of-flight measurements in the calorimeter as in sec.2. Additional kinematical cuts have been applied to reduce background further: on i) the $(\theta_{+\gamma}, \theta_{-\gamma})$ plane, the angle between $\pi^+(\pi^-)$ and the closest photon from π^0 decay; ii) on the angle between clusters in the π^0 rest frame, $\theta_{\gamma\gamma}^* > 165^\circ$ and iii) on the the missing mass squared, $P_{\pi^0}^2, ||P_{\pi^0} - m_{\pi^0}| < 15 \text{ MeV}$.

Signal selection efficiency is 37.6% and signal to background ratio, evaluated from a fit to MC-corrected shape of all components, is S/N=133[15]. The bin width of the Dalitz plot is determined both, by the resolution in x and y , and the number of events in each bin. In the analysis we used 31 and 20 bins respectively for x and y , achieving a minimal bin content of $3.3 \cdot 10^3$ events. The fit is performed by minimizing the function,

$$\chi^2 = \sum_{i=1}^n \left(\frac{N_i - \sum_{j=1}^{n_T} S_{ij} N_{T,j}}{\sigma_i} \right)^2 \quad (4.2)$$

where $N_{T,j} = \int |A(X, Y)|^2 d\Phi(X, Y)_j$ is the integral on the phase space of the j -th bin; $N_i = N_{data,i} - N_{bck,i}$ is the background-subtracted content of the i -th bin; S_{ij} is acceptance and smearing matrix from bin j to bin i , as determined by MC studies; $\sigma_i^2 = \sigma_{N_i}^2 + \sigma_{S_{ij}}^2$ is the error in each bin. fig. 3, shows data distribution after background subtraction and the distribution of normalized residuals between χ^2 and χ^2_{min} .

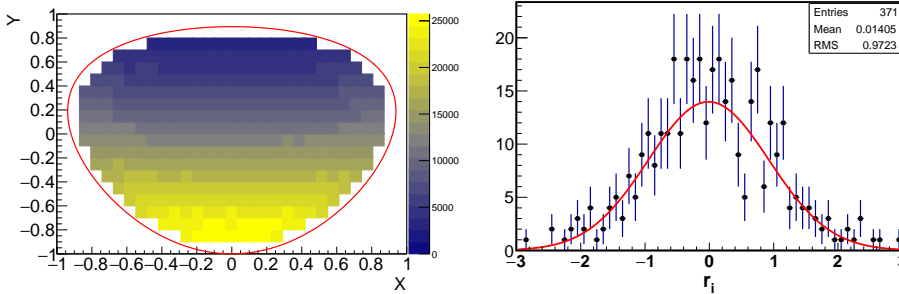


Figure 3: On the left, experimental background-subtracted Dalitz plot data. On the right, normalized residuals for the 137 bins obtained from the fit to data.

Final results for the Dalitz plot parameters, after a careful study of all systematic effects, are: $a = -1.104 \pm 0.003 \pm 0.002$, $b = +0.142 \pm 0.003^{+0.005}_{-0.004}$, $d = +0.073 \pm 0.003^{+0.004}_{-0.003}$, $f = +0.154 \pm$

$0.006_{-0.005}^{+0.004}$, in agreement with, and a factor from 2–3 more precise than previous measurements. Recently [16] calculate the parameter-free predictions obtained from the neutral Dalitz plot and the neutral-to-charged branching ratio $Q = 22.0 \pm 0.7$, using the remarkably precise result for the ratio $m_s/m_{ud} = 27.30 \pm 34$ from lattice [17], the authors [16] can finally also determine the relative size of the two lightest quark masses: $m_u/m_d = 0.44 \pm 0.03$.

References

- [1] Amelino-Camelia G., *et al.*, **Physics with the KLOE-2 experiment at the upgraded DAΦNE**, *Eur. Phys. J. C* **68**, 2010, 619;
- [2] Terschlusen C. and Leupold S., **Electromagnetic Transition Form Factors of Mesons**, *Prog. Part. Nucl. Phys.* **67**, 2012, 401;
- [3] Schneider S. P., Kubis B. and Niecknig F., **The $\omega^- \rightarrow \pi^0 \gamma^*$ and $\phi^- \rightarrow \pi^0 \gamma^*$ transition form factors in dispersion theory**, *Phys. Rev. D* **86**, 2012, 054013;
- [4] Jegerlehner F., and Nyffeler A., **The Muon g-2**, *Phys. Rept.*, **477**, 2009, 1;
- [5] Anastasi, A. *at al.*, **Measurement of the $\phi \rightarrow \pi^0 e^+ e^-$ transition form factor with the KLOE detector**, *Phys. Lett. B* **757**, (2016), 362;
- [6] Ambrosino, F. *at al.*, **Measurement of the DAFNE luminosity with the KLOE detector using large angle Bhabha scattering**, *Eur. Phys. J. C* **47**, (2006), 589;
- [7] Olive K. A., *Review of Particle Physics C* **40**, (2016), 100001;
- [8] Ivashyn S., **Vector to pseudoscalar meson radiative transitions in chiral theory with resonances**, *Prob. Atomic Sci. Technol.* **2012N1**, (2012), 179;
- [9] Danilkin I. V. *at al.*, **Dispersive analysis of $\omega/\phi \rightarrow 3\pi, \pi\gamma^*$** , *Phys. Rev. D* **91**, (2015), 094029;
- [10] Babusci D. *et al.*, **Study of the Dalitz decay $\phi \rightarrow \eta e^+ e^-$ with the KLOE detector"**, *Phys. Lett. B*, **742**, (2015), 1;
- [11] Faessler A. Fuchs C. and Krivoruchenko M. I., **Dilepton spectra from decays of light unflavored mesons**, *Phys Rev. C*, **61**, (2000), 035206;
- [12] Akhmetshin R. R. *at al.*, **Study of conversion decays $\phi \rightarrow \eta e^+ e^-$, $\eta \rightarrow e^+ e^- \gamma$ and $\eta \rightarrow \pi^+ \pi^- e^+ e^-$ at CMD-2**, *Phys. Lett. B*, **501**, (2001), 191;
- [13] Achasov M. N. *at al.*, **Study of Conversion Decays $\phi \rightarrow \eta e^+ e^-$ and $\eta \rightarrow \gamma e^+ e^-$ in the Experiment with SND Detector at the VEPP-2M Collider**, *Phys. Lett. B*, **504**, (2001), 275;
- [14] Kolesar M. and Novotny J. **Convergence properties of $\eta \rightarrow 3\pi$ decays in chiral perturbation theory** *hep-ph:1607.00338*
- [15] Anastasi A. *et al.*, **Precision measurement of the $\eta \rightarrow \pi^+ \pi^- \pi^0$ Dalitz plot distribution with the KLOE detector**, *JHEP* **05**, (2016), 019;
- [16] Colangelo $\eta \rightarrow 3\pi$ **Study of the Dalitz Plot and Extraction of the Quark Mass Ratio Q**, *G. et al. Phys Rev. Lett.* **118**, (2017), 022001;
- [17] S. Aoki *et al.*, **Review of lattice results concerning low-energy particle physics** arXiv:1607.00299.